

Influence of extraction voltage on electron and ion behavior characteristics

Ao Xu(徐翱), Pingping Gan(甘娉娉), Yuanjie Shi(石元杰), and Lei Chen(陈磊)

Citation: Chin. Phys. B, 2024, 33 (**4**): 045203. DOI: 10.1088/1674-1056/ad1820
Journal homepage: http://cpb.iphy.ac.cn; http://iopscience.iop.org/cpb

What follows is a list of articles you may be interested in

Plasma potential measurements using an emissive probe made of oxide cathode

Jian-Quan Li(李建泉), Hai-Jie Ma(马海杰), and Wen-Qi Lu(陆文琪)
Chin. Phys. B, 2024, 33 (**4**): 045205. DOI: 10.1088/1674-1056/ad1821

Numerical studies for plasmas of a linear plasma device HIT-PSI with geometry modified SOLPS-ITER

Min Wang(王敏), Qiuyue Nie(聂秋月), Tao Huang(黄韬), Xiaogang Wang(王晓钢), and Yanjie Zhang(张彦杰)
Chin. Phys. B, 2024, 33 (**3**): 035204. DOI: 10.1088/1674-1056/ad16d4

Wave field structure and power coupling features of blue-core helicon plasma driven by various antenna geometries and frequencies

Chao Wang(王超), Jia Liu(刘佳), Lei Chang(苌磊), Ling-Feng Lu(卢凌峰), Shi-Jie Zhang(张世杰), and Fan-Tao Zhou(周帆涛)
Chin. Phys. B, 2024, 33 (**3**): 035201. DOI: 10.1088/1674-1056/ad1486

Differences between two methods to derive a nonlinear Schrödinger equation and their application scopes

Yu-Xi Chen(陈羽西), Heng Zhang(张恒), and Wen-Shan Duan(段文山)
Chin. Phys. B, 2024, 33 (**2**): 025203. DOI: 10.1088/1674-1056/ad082b

Transition from a filamentary mode to a diffuse one with varying distance from needle to stream of an argon plasma jet

Hui-Min Xu(许慧敏), Jing-Ge Gao(高敬格), Peng-Ying Jia(贾鹏英), Jun-Xia Ran(冉俊霞), Jun-Yu Chen(陈俊宇), and Jin-Mao Li(李金懋)
Chin. Phys. B, 2024, 33 (**1**): 015205. DOI: 10.1088/1674-1056/ad0149

Influence of extraction voltage on electron and ion behavior characteristics

Ao Xu(徐翱), Pingping Gan(甘娉娉)†, Yuanjie Shi(石元杰), and Lei Chen(陈磊)

Institute of Electronic Engineering, China Academy of Engineering Physics, Mianyang 621999, *China*

(Received 25 October 2023; revised manuscript received 15 December 2023; accepted manuscript online 22 December 2023)

The characteristics of the extracted ion current have a significant impact on the design and testing of ion source performance. In this paper, a 2D in space and 3D in velocity space particle in cell (2D3V PIC) method is utilized to simulate plasma motion and ion extraction characteristics under various initial plasma velocity distributions and extraction voltages in a Cartesian coordinate system. The plasma density is of the order of 10^{15} m^{-3}–10^{16} m^{-3} and the extraction voltage is of the order of 100 V–1000 V. The study investigates the impact of various extraction voltages on the velocity and density distributions of electrons and positive ions, and analyzes the influence of different initial plasma velocity distributions on the extraction current. The simulation results reveal that the main reason for the variation of extraction current is the space-charge force formed by the relative aggregation of positive and negative net charges. This lays the foundation for a deeper understanding of extraction beam characteristics.

Keywords: extraction voltage, plasma, ion beam, ion current

PACS: 52.65.–y, 52.65.Rr, 29.25.–t, 29.25.Ni **DOI:** 10.1088/1674-1056/ad1820

1. Introduction

In many plasma applications, the plasma produced by a discharge will pass through a diffusion region and then positive ions are extracted.[1,2] The ion extraction characteristics in this process have attracted the attention of researchers. The plasma density (of the order of 10^{15} m^{-3}–10^{18} m^{-3}) and distribution, extraction voltage (of the order of 100 V to 100 kV) and extracted ion beam intensity (of the order of 1 μA to 100 mA) and its distribution are important parameters of most concern. Kosonen investigated the applicability of the Child–Langmuir (CL) law to ion source extraction and indicated that the CL law is not valid for the total beam current but instead requires collimation for the emergence of the CL effect.[3] Li and Sun presented a two-dimensional (2D) hybrid model to simulate the ion optics for positive ion extraction and demonstrated that the thermal velocities of ions can affect the perveance condition of the ion beams.[4] Abadi and Mahjour-Shafiei demonstrated the correlation between the emittance of the He^+ beam extracted from a cold cathode Penning ion source and the source voltage, anode length and cathode-to-anode distance using 2D in space and 3D in velocity space particle in cell (2D3V PIC) Monte Carlo simulations.[5] Abdelrahman discussed the principles of plasma generation and ion extraction from various types of ion sources. He also presented the theory of ion focusing, along with some examples of electrostatic focusing systems.[6] Soliman *et al*. optimized the extraction and focusing system of the ion beam without any losses by using the SIMION 3D code. Additionally, they described the possible plasma boundary curvatures during ion extraction.[7] Dorf *et al*. investigated the relationship between the extracted beam current and plasma density, and suggested that beam formation in the plateau regime could suppress noise and stabilize the extracted current.[8] Keller observed the process of ion beam formation and the extraction system for high-current beams extracted from plasma ion sources. He developed a general scaling model for extraction systems that can be applied to a wide range of beam current and energy values.[9] The space-charge-limited current[10–12] and plasma sheath[13–16] related to ion extraction have also received widespread attention. These studies mainly focused on the changes in ion emission surface, the intensity and distribution characteristics of the extracted beam under acceleration voltages of tens or even hundreds of kV, as well as the sheath characteristics formed by the interaction between plasma and the wall. There are few studies on the characteristics of the extracted ion beam at lower voltages; however, ion current measurements of ion sources often use lower extraction voltages. Therefore, it is necessary to study the plasma diffusion and ion extraction characteristics under these lower-voltage conditions.

In this paper, a 2D3V PIC code[17,18] is utilized to establish a simulation model of plasma diffusion and ion beam formation under different extraction voltages. The impact of different extraction voltages on the motion behavior of electrons and positive ions is analyzed. The similarities and differences in the velocity, density and current of charged particles in the extraction ion beam under different initial plasma velocity distributions and extraction voltages are discussed, as well

†Corresponding author. E-mail: ganpingping@caep.cn

© 2024 Chinese Physical Society and IOP Publishing Ltd

as the reasons for the differences.

2. Simulation model

Based on the 2D3V PIC method, a simulation model for plasma diffusion and extraction is established. A schematic diagram of the model is shown in Fig. 1. The model consists of a plasma chamber (including grids) and an extraction electrode, all made of metal. The plasma chamber and grid are grounded, the extraction electrode is connected with a negative voltage, and the areas without electrodes on both sides are set as the Neumann boundary condition. The calculated area is 5 mm × 5 mm. The wall thickness, inner length and width of the plasma chamber are 0.1 mm, 4.8 mm and 2.5 mm, respectively. The grid has a length of 0.05 mm and a width of 0.1 mm. The distance between the plasma chamber and the extraction electrode is 2.4 mm, and the plasma injection area is 1 mm long.

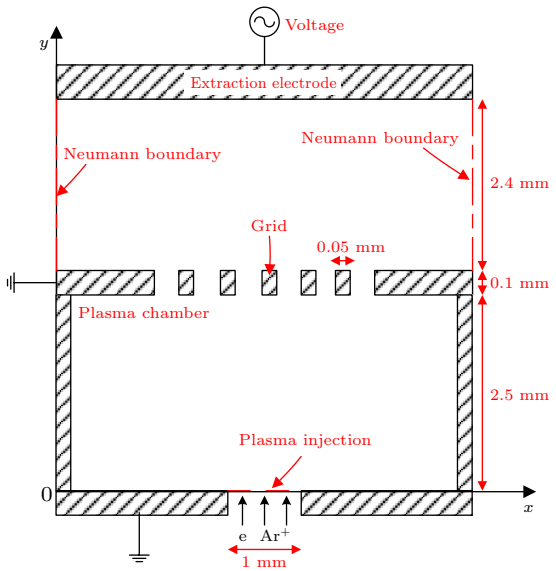


Fig. 1. Schematic diagram of the simulation model (not to scale).

As Ar is a relatively safe inert gas commonly used in many experimental discharge cavities we used it in our simulations. The simulated particles are electrons and Ar^+, and the secondary electron effect resulting from particle bombardment on the device wall is not taken into account. In the plasma injection area, the flux of the electrons is set as 1×10^{21} $m^{-2}{\cdot}s^{-1}$ with a temperature of 5.0 eV and average velocity of 1×10^5 $m{\cdot}s^{-1}$, and the flux of Ar^+ is set as 1×10^{20} $m^{-2}{\cdot}s^{-1}$ with a temperature of 0.1 eV and average velocity of 1×10^4 $m{\cdot}s^{-1}$. These parameters refer to the experimental results for our gas discharge ion source. It should be noted that the initial velocities of all particles are in the Y direction. Two types of initial plasma (electrons and ions) velocity distributions are considered in the simulation. The uniform distribution implies that all electrons and ions have the same initial velocity of 1×10^5 $m{\cdot}s^{-1}$ and 1×10^4 $m{\cdot}s^{-1}$ in the Y direction, respectively. The Maxwellian distribution means that the velocities of the electrons and ions follow a local Maxwellian distribution around the average velocities of 1×10^5 $m{\cdot}s^{-1}$ and 1×10^4 $m{\cdot}s^{-1}$ in the Y direction, respectively. The time step and space step are 10^{-12} s and 0.025 mm, respectively.

After numerous rounds of simulation and comparison, we found that the simulation results converge steadily at 3 μs, as depicted in Fig. 2. Therefore, the results at 3 μs are discussed in the following sections.

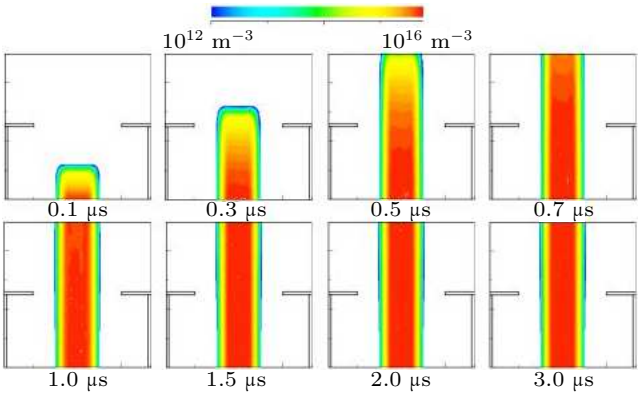


Fig. 2. Ion density distribution at different times.

3. Simulation results for uniform distribution of injected plasma velocity

Based on the simulation model in the previous section, and setting a uniform distribution of injected plasma velocity, the extraction electrode is connected with voltages of 1×10^{-6} V (close to 0 V, because the code does not allow a direct setting of 0 V), −10 V, −50 V, −100 V, −200 V, −500 V, −1000 V and −5000 V. The density distributions of electrons and Ar^+ under different extraction voltages at 3 μs are obtained by simulation, as shown in Figs. 3 and 4.

It can be seen from Fig. 3 that when the extraction voltage is about 0 V, the electrons mainly move vertically toward the extraction electrode. Due to the space-charge force, a small number of electrons will be repelled and escape to both sides, causing the electrons to fill the whole simulation area. As the amplitude of the extraction voltage increases, the negative extraction voltage suppresses the electrons outside the plasma chamber, resulting in virtually no electrons escaping outside the plasma chamber. As the amplitude of the extraction voltage increases, the electric field entering the plasma chamber also increases, leading to a decrease in the number of escaping electrons in the chamber. Furthermore, the distance that the main electron beam can travel to the extraction electrode also decreases with increase in the extraction voltage amplitude. When the extraction voltage amplitude is 500 V, the main electron beam starts to be confined in the plasma chamber, and when the extraction voltage amplitude is increased to

5000 V, the main electron beam can only travel halfway across the width of the plasma chamber.

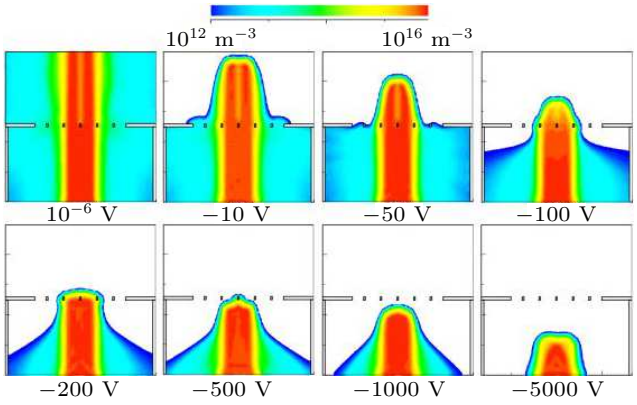


Fig. 3. Electron density distribution under different extraction voltages.

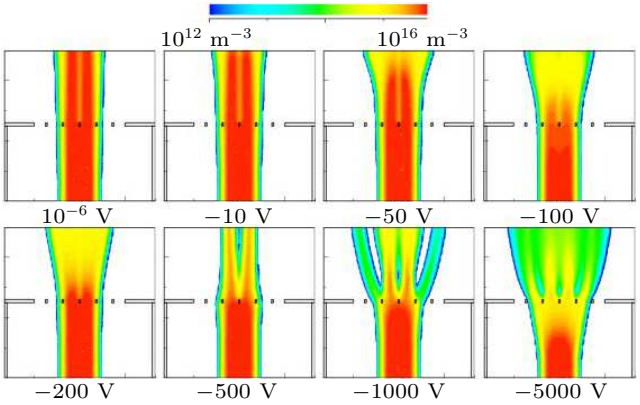


Fig. 4. Ion density distribution under different extraction voltages.

As can be seen from Fig. 4, when the amplitude of the extraction voltage is no greater than 200 V, the extraction voltage has minimal impact on the Ar^+ ion beam within the plasma chamber. However, outside the plasma chamber, the Ar^+ ion beam diverges as the extraction voltage amplitude increases. This divergence occurs because the extraction voltage hinders electrons, causing them to travel a shorter distance to the extraction electrode as the extraction voltage amplitude increases. In other words, electrons separate from positive ions at an earlier stage. When the Ar^+ ion beam continues to move forward after losing electrons, its own space-charge force will cause the ion beam to continuously diverge. The earlier it separates from electrons, the greater the degree of divergence. Through the simulation results of potential distribution at the grid ($y = 2.6$ mm) under the condition of an extraction voltage amplitude of 100 V–500 V, as shown in Fig. 5, it can be observed that even if the extraction voltage amplitude reaches 500 V, the potential that can penetrate into the plasma chamber is only about 20 V and the electrons and positive ions are separated just near the grid, which in turn leaves the distribution of the Ar^+ ion beam in the plasma chamber unaffected due to the small penetration electric field. However, the formation of multiple concave distributions at the grid potential, despite its small value, results in the creation of a focusing electric field force between the grid and the extraction electrode. This causes the region with a relatively low edge density of the extracted Ar^+ ion beam to shrink due to focusing of the electric field force during movement. When the amplitude of the extraction voltage is 1000 V or more, the electric field penetrates the plasma chamber, causing the electrons and positive ions to separate. As a result, the Ar^+ ion beam in the plasma chamber starts to diverge, leading to it reaching the grid with not just the y-direction velocity, especially at the edge of the beam current. At this time, despite the presence of a focusing electric field force between the grid and the extraction electrode, the Ar^+ ion beam will still diverge.

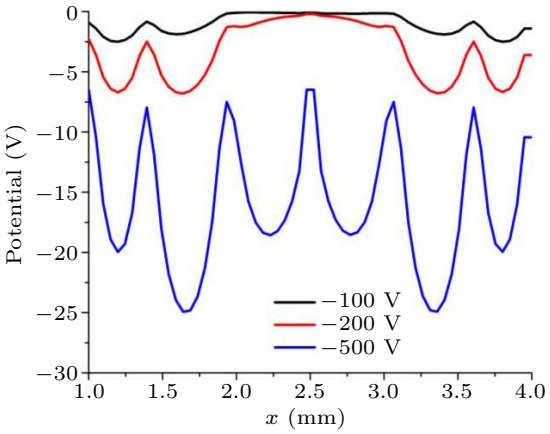


Fig. 5. Potential distribution at the grid under different extraction voltages.

The distributions of Ar^+ density and velocity (the scalar of the total velocity) at the grid ($y = 2.6$ mm) under the condition of an extraction voltage amplitude of 500 V–5000 V are shown in Figs. 6 and 7. It can be seen that with the increase in extraction voltage amplitude, the Ar^+ density at the grid decreases and the velocity increases. The increase in Ar^+ velocity is due to enhancement of the electric field resulting from the increase in extraction voltage amplitude, which accelerates Ar^+. The density of Ar^+ decreases continuously, because under these conditions electrons are continuously compressed with increase in the extraction voltage in the plasma chamber, resulting in positive and negative charges being relatively concentrated in the plasma movement path in the plasma chamber. The net charge distribution (when the extraction voltage amplitude is 5000 V) is shown in Fig. 8. The positive charges are concentrated in the plasma motion path in the middle of the plasma chamber, and the negative charges are concentrated below it. This leads to a change in the motion of Ar^+ when moving through the negative charge accumulation region due to the similar 'virtual anode' created by the accumulation of positive charges, resulting in the repulsion of Ar^+ by the local electric field force. The local electric field distribution ($x = 1$ mm–4 mm, $y = -2$ mm, when the voltage amplitude is 5000 V) is shown in Fig. 9. It can be observed that many newly implanted Ar^+ ions will be repelled by the local electric

field force in the direction opposite to their movement, leading to a decrease in the density of Ar^+ ions reaching the grid. Furthermore, as the extraction voltage amplitude increases, the compression of the electron distribution becomes more pronounced, and the repulsion from the 'virtual anode' formed by positive charge aggregation becomes more evident. When the positive charge aggregates above the plasma implantation area, and a large number of positive ions cannot be implanted, it reaches equilibrium.

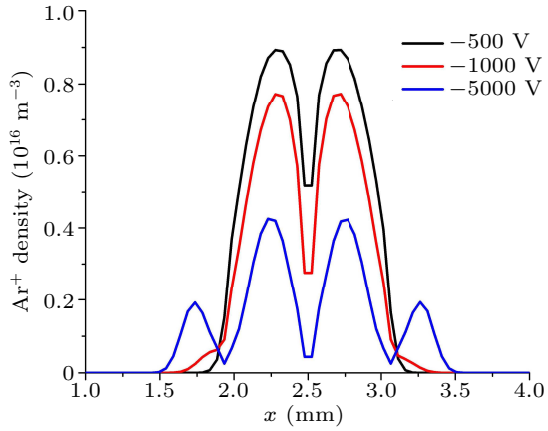


Fig. 6. Ion density distribution at the grid under different extraction voltages.

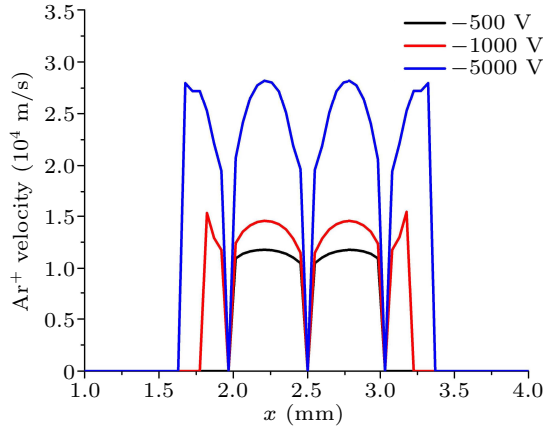


Fig. 7. Ion velocity distribution at the grid under different extraction voltages.

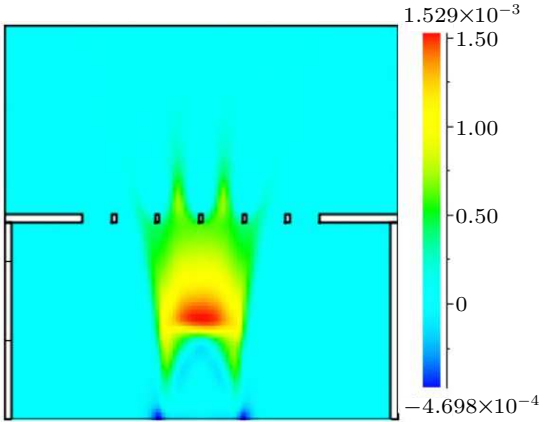


Fig. 8. Net charge distribution with an extraction voltage of −5000 V (the unit for the color bar is Coulomb).

Since a two-dimensional simulation cannot directly obtain the Ar^+ ion beam current only the current density distribution can be calculated. Assuming that the simulation results within 1 mm perpendicular to the simulation area are the same, the Ar^+ ion beam current can be calculated for different extraction voltages. As shown in Fig. 10, although the extraction voltage can affect the density and velocity distribution of the Ar^+ ion beam, increase in the Ar^+ velocity counteracts the decrease in its density. The different extraction voltages have no obvious effect on the extraction Ar^+ ion beam current.

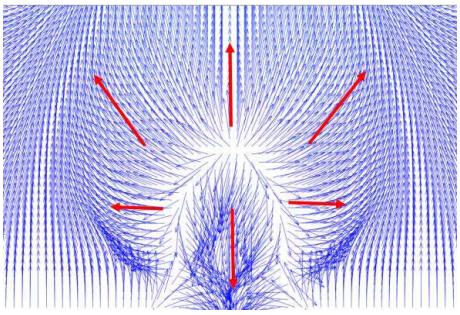


Fig. 9. Electric field vector distribution in areas of $x = 1$ mm–4 mm and $y = 0$ mm–2 mm.

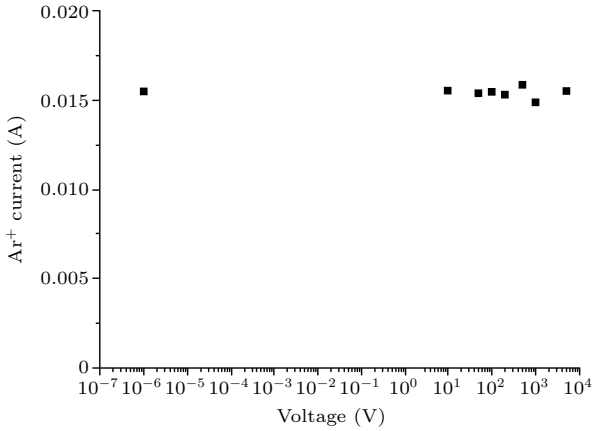


Fig. 10. Ion current under different extraction voltages.

4. Simulation results for Maxwellian distribution of injected plasma velocity

Using the same simulation model, the injected electron velocity is changed to a Maxwellian distribution. The electron and Ar^+ density distributions under different extraction voltages at 3 μs are shown in Figs. 11 and 12, respectively.

It can be seen from Fig. 11 that, unlike the previous condition of uniform initial plasma velocity, when the initial plasma velocity follows a Maxwellian distribution, electron divergence occurs outside the plasma chamber in the range of 0–5000 V. This might be caused by a space-charge force formed by the uneven velocity inside the plasma. Furthermore, there is no discernible disparity in the maximum distance that electrons can travel under two distinct initial plasma velocity distributions, despite varying extraction voltages.

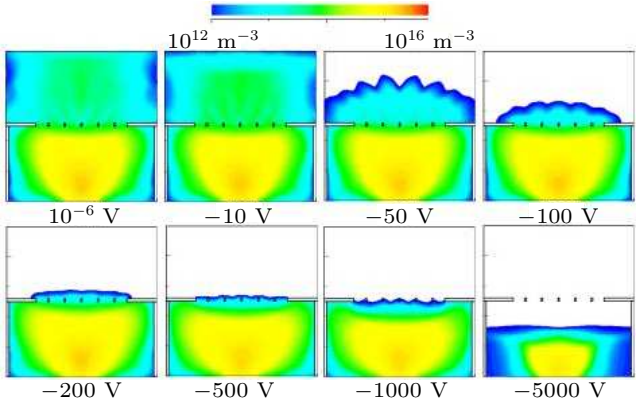


Fig. 11. Electron density distribution under different extraction voltages.

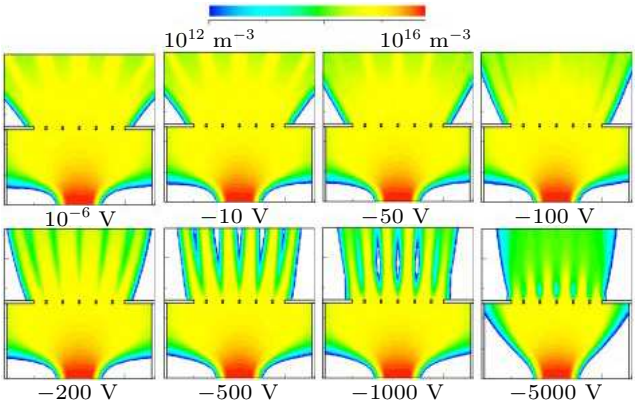


Fig. 12. Ion density distribution under different extraction voltages.

Comparing Figs. 12 and 4, it can be seen that the distribution characteristics of the Ar^+ ion beam are significantly different under two distinct initial plasma velocity distributions. For a Maxwellian distribution of initial plasma velocity, Ar^+ occupies most of the region in the plasma chamber when the amplitude of the extraction voltage does not exceed 1000 V. This is attributed to the divergence of electrons in the chamber when the voltage amplitude is below 1000 V, causing Ar^+ to diverge under the influence of the space-charge force. When the amplitude of the extraction voltage is increased to 5000 V, the distribution of Ar^+ in the plasma chamber decreases, but it remains significantly larger than that for a uniformly distributed initial plasma velocity. The reduction in the Ar^+ distribution is caused by the accumulation of electrons under an extraction voltage of −5000 V. Outside the plasma chamber, as the amplitude of the extraction voltage increases, the distribution of Ar^+ continuously decreases.

Comparing the simulation results of potential distribution at the grid ($y = 2.6$ mm) with a voltage amplitude of 100 V–500 V under the two different initial plasma velocity distributions, as shown in Figs. 5 and 13, there is no obvious difference in potential distribution between the two conditions except for a slight difference in potential near the center ($x = 2.5$ mm).

The Ar^+ density and velocity (the scalar of the total velocity) distribution at the grid ($y = 2.6$ mm) under extraction voltage amplitudes of 500 V–5000 V are shown in Figs. 14 and 15. The Ar^+ velocity increases with increase in the extraction voltage amplitude under two different initial plasma velocity distributions, and the maximum Ar^+ velocity in the two cases is about 28000 m·s^{-1} for an extraction voltage amplitude of 5000 V. However, when the initial plasma velocity has a Maxwellian distribution, the Ar^+ density distribution changes little with the extraction voltage, which is completely different from the decrease of Ar^+ density with increase in the extraction voltage amplitude when the initial plasma velocity is uniform. The net charge distribution with an initial Maxwellian plasma velocity distribution under an extraction voltage of −5000 V is shown in Fig. 16. Many electrons have X-direction velocity components due to the divergence of electrons in the plasma chamber, which leads to many electrons moving to both sides when the electric field penetrates the plasma chamber and presses electrons, making the negative charge-gathering region appear on both sides of the positive charge-gathering region. The local electric field distribution under an extraction voltage amplitude of 5000 V is shown in Fig. 17. The electric field force formed by the relative aggregation of positive and negative charges does not impede the movement of Ar^+ ions. Therefore, the density of Ar^+ entering the plasma chamber and being extracted will not decrease significantly with increase in the amplitude of the extraction voltage.

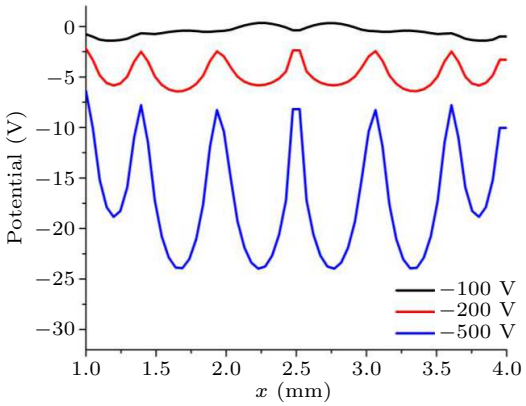


Fig. 13. Potential distribution at the grid under different extraction voltages.

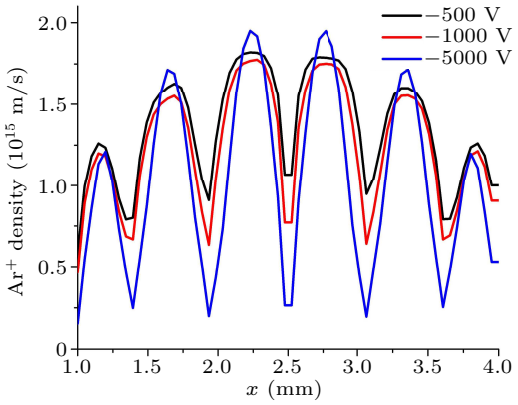


Fig. 14. Ion density distribution at the grid under different extraction voltages.

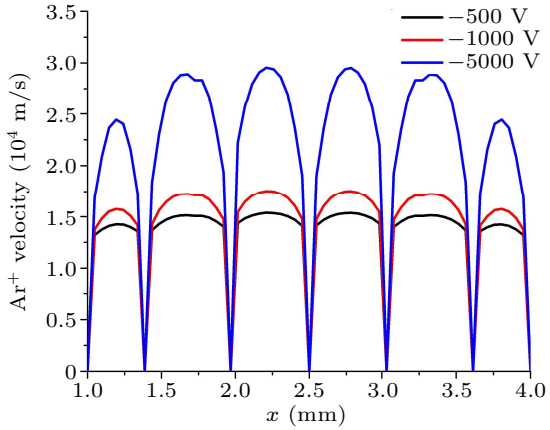


Fig. 15. Ion velocity distribution at the grid under different extraction voltages.

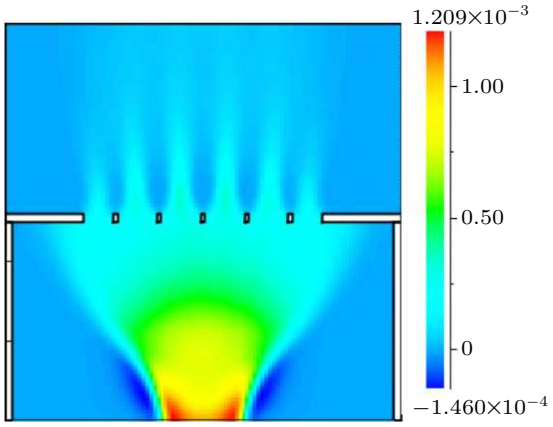


Fig. 16. Net charge distribution with an extraction voltage of −5000 V (the unit for the color bar is Coulomb).

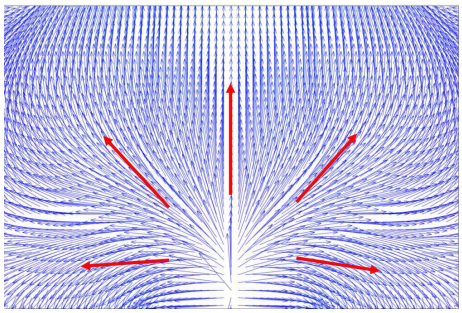


Fig. 17. Electric field vector distribution in the area $x = 1$ mm–4 mm and $y = 0$ mm–2 mm.

Finally, the Ar^+ ion beam current under different extraction voltages can be calculated using the method mentioned in the previous section. As depicted in Fig. 18, the Ar^+ ion beam current remains unaffected by changes in the extraction voltage amplitude when the amplitude is 500 V or less. However, when the extraction voltage amplitude exceeds 1000 V, the Ar^+ ion beam current increases with increase in the extraction voltage amplitude. This is attributed to the increase in extraction speed and the nearly constant Ar^+ density.

In reality, the initial velocity of particles produced by an ion source cannot be completely evenly distributed, and a Maxwellian distribution of initial particle velocity is more consistent with the actual situation. In other words, for actual ion extraction, when the voltage meets specific conditions the extraction current will increase as the voltage amplitude increases.

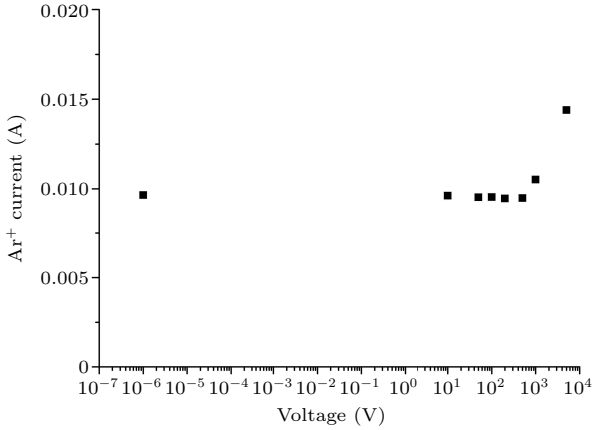


Fig. 18. Ion current under different extraction voltages.

5. Conclusions

In this paper, the 2D3V PIC code is utilized to simulate the impact of varying voltages on the distribution of electrons, positive ions and the ion beam current under different initial plasma velocity distributions. When the initial plasma velocity is uniform, the density and velocity distribution of electrons and positive ions will change with change in the extraction voltage. However, the extraction current of ions is essentially unaffected by the change in extraction voltage. When the initial plasma velocity has a Maxwellian distribution, the diffusion of electrons and positive ions is more pronounced than when the initial plasma velocity has a uniform distribution. The ion extraction current increases as the extraction voltage amplitude increases, but only when the amplitude of the extraction voltage exceeds 1000 V. This is due to the Maxwellian distribution of the initial plasma velocity, which results in the formation of a space-charge force and electron divergence. As a result, electrons and ions do not accumulate in the plasma path, thereby preventing the obstruction of the movement of positive ions. The density of positive ions does not decrease significantly with increase in the extraction voltage amplitude. However, the velocity of positive ions increases with increase in extraction voltage amplitude, leading to an increase in ion current. All these factors help us to better understand the current characteristics of the extracted ions.

Acknowledgments

Project supported by Presidential Foundation of CAEP (Grant No. YZJJZQ2022016) and the National Natural Science Foundation of China (Grant No. 52207177).

References

[1] Abdelrahman M M, Basal N I and Zakhary S G 2012 *Chin. Phys. C* **36** 344

[2] Wolf B 1995 *Handbook of Ion Sources* (Boca Raton: CRC Press)

[3] Kosonen S T, Kalvas T, Tarvainen O and Toivanen V 2022 *J. Phys.: Conf. Ser.* **2244** 12079

[4] Li H L and A B Sun 2021 *Comput. Phys. Commun.* **259** 0107629

[5] Abadi M R N and Mahjour-Shafiei M 2021 *Rev. Sci. Instrum.* **92** 123501

[6] Abdelrahman M M 2012 *Ain Shams Engineering Journal* **3** 71

[7] Soliman B A, Abdelrahman M M, Helal A G and Abdelsalam F W 2011 *Chin. Phys. C* **35** 83

[8] Dorf M A, Sidorov A V, Zorin V G, Bohanov A F, Vodopyanov A V, Izotov I V, Razin S V and Skalyga V A 2007 *J. Appl. Phys.* **102** 054504

[9] Keller R 1990 *Nuclear Instruments and Methods in Physics Research A: Accelerators, Detectors, Associated Equipment* **298** 247

[10] Garner A L, Darr A M and Harsha N R S 2022 *IEEE Trans. Plasma Sci.* **50** 2528

[11] Huang H and Liu Y J 2019 *IEEE Trans. Plasma Sci.* **47** 3631

[12] Lafleur T and Aanesland A 2014 *Phys. Plasmas* **21** 123506

[13] Benilov M S 2009 *Plasma Sources Sci. Technol.* **18** 014005

[14] Masamune S and Yukimura K 2006 *IEEE Trans. Plasma Sci.* **34** 1195

[15] Mandl S, Gunzel R and Moller W 1998 *J. Phys. D: Appl. Phys.* **31** 1109

[16] Baalrud S D, Scheiner B, Yee B T, Hopkins M M and Barnat E 2020 *Plasma Sources Sci. Technol.* **29** 053001

[17] Su Y, Li J, Wang H and Xu A 2021 *IEEE Trans. Plasma Sci.* **49** 1214

[18] Li J, Yang F, Fan Z, Du W and Xu A 2022 *IEEE Trans. Plasma Sci.* **50** 1097